Journal of Power Sources, *13* (1984) 297 - 318

A COMPARATIVE STUDY OF THE EFFECTS OF SURFACE CONDITION AND AMALGAMATION ON THE CORROSION AND POLARISATION CHARACTERISTICS OF PURE ZINC AND TWO BATTERY ZINC ALLOYS IN LECLANCHE RELATED ELECTROLYTE

L. M. BAUGH and A. HIGGINSON*

Ever Ready Ltd., Technical Division, Tanfield Lea, Stanley, Co. Durham DH9 9QF (U.K.)

(Received June 18, 1984)

Summary

The effect of surface preparation and amalgamation on the corrosion and polarisation characteristics of pure zinc and two battery zinc alloys (Zn–Pd–Cd) and (Zn–Pb–Cd–Fe) has been compared and contrasted in concentrated NH_4Cl solution. Polished metal surfaces have been used to simulate the surface condition of the anode materials during initial battery storage periods and etched surfaces have been used to simulate conditions after high rate discharge. The investigation highlights the extreme sensitivity of the corrosion behaviour to small changes in regard to the high (Pb, Cd) or low (Fe) hydrogen overvoltage components. In order to explain the corrosion characteristics of the etched alloys consideration must be given to the effect of surface accumulation of minor alloying constituents in addition to surface roughness changes. Amalgamation of the polished specimens produces a significant reduction in their corrosion rate. Amalgamation of the etched metals removes the effect of the accumulated minor alloying components Pb and Cd, probably by surface amalgam formation. In the case of the Fe containing alloy, however, the deleterious effects of the surface accumulation of Fe cannot be removed.

Introduction

Although zinc is used as the anode material in a wide variety of primary batteries, it is only comparatively recently that the corrosion and polarisation characteristics of this metal have been systematically examined in relevant electrolyte systems. These investigations have involved studies of the corrosion behaviour of zinc in neutral/acid media [1, 2], the pitting characteristics of zinc in Leclanché and related electrolytes [3, 4], and the effect of amalgamation on the corrosion and polarisation characteristics of zinc in

*Present address: Council for Mineral Technology, Randburg, South Africa 2125.

0378-7753/84/$3.00

battery electrolyte analogues [5, 6]. To facilitate an understanding of the basic corrosion mechanisms, pure zinc electrodes were predominantly utilised in these studies [1, 5, 6]. Practical anode materials, particularly in the case of Leclanché batteries, however, are invariably zinc alloys.

In this paper we present the results of an examination of the corrosion and polarisation characteristics of two such alloy systems (Zn–Pb–Cd) and (Zn–Pb–Cd–Fe) which are compared and contrasted with those of pure zinc to reveal specific contributions from the minor alloying constituents Pb, Cd, and Fe. It is emphasised that a detailed quantitative surface analysis of the electrodes was beyond the scope of the present investigation, which was undertaken principally to define the main *trends* in the electrochemical and corrosion parameters.

The composition of the zinc alloy cup used in Leclanché batteries is dictated by metallurgical considerations. Lead is added as a *grain refiner*, reducing the grain size to a level which facilitates acceptable and consistent extrusion characteristics. It also prevents deep penetration of the mercury in the amalgamation process, alleviating the likelihood of cup perforation and ensuring a high concentration of mercury at the zinc surface exposed to the electrolyte. Cadmium is added to the zinc as a *hardener* which imparts sufficient strength to the extruded cup to withstand resistance to distortion during battery assembly.

The third metal of importance is iron which is used as a *high temperature grain stabiliser*, preventing grain growth during certain anode processing stages employing high temperatures ($\geqslant$200 °C).

Clearly, the choice of Pb and Cd as agents for controlling grain size and hardness, respectively, has been influenced by the fact that these metals do not evolve hydrogen as easily as does zinc and, therefore, they impart a degree of corrosion protection. Iron additions, however, do not give such corrosion resistance and, by contrast, accelerated corrosion is expected.

In order to magnify the deleterious or beneficial effects of minor alloying constituents in the present investigation, corrosion and polarisation measurements have been made on etched metal surfaces as well as on polished surfaces. The etching process, although producing an increase in surface roughness, concentrates the minor alloying components at the metal surface; a process which also occurs during anodic discharge. Since battery zinc is amalgamated to facilitate a low corrosion rate, amalgamated electrodes have also been studied. Scanning electron microscopy has been used to observe and characterise the metal surface textures and obtain information as to the surface distribution of minor alloying constituents and mercury. Electron probe microanalysis of the etched surfaces has also been carried out.

Experimental

The three working electrodes used in the present work were pure zinc (99.999% supplied by Koch-Light), a Zn–Pb–Cd alloy (Zn–0.8%Pb–

0.06%Cd) and a Zn–Pb–Cd–Fe alloy (Zn–0.2%Pb–0.08%Cd–0.014%Fe). These electrode materials, in the form of rods (circular cross-sectional area 0.283 cm^2), were sheathed in tightly fitting Teflon and polished in the manner described previously. Electrodes were etched, if necessary, for 1 min in 15% HCl at a rotation speed of 20 Hz. They were then thoroughly rinsed in triply-distilled water. Amalgamation was accomplished by electrolytic deposition of mercury from 1M KOH saturated with yellow HgO. About 20 μg of Hg cm^{-2} was reproducibly deposited. The amalgamated electrodes were thoroughly rinsed in deoxygenated, triply distilled water before being transferred to the polarisation cell.

The electrochemical cell, instrumentation and procedure have been described previously [1]. The cell and electrode assemblies were situated inside a thermostatically controlled enclosure at 30 ± 0.1 °C. The working electrolyte was 6.0 mol cm^{-3} of NH_4Cl prepared from AnalaR grade salt and thrice distilled water. The reference electrode was $Hg/Hg_2Cl_2/KCl$ (sat).

Corrosion currents were determined by the Tafel line extrapolation and polarisation resistance methods [1]. All experiments were duplicated and conducted under de-aerated conditions.

Results and discussion

(i) Electron microscopy

Figures 1 - 3 show optical and scanning electron micrographs of the pure zinc, (Zn–Pb–Cd), and (Zn–Pb–Cd–Fe) electrode surfaces, respectively, prior to the electrochemical measurements. In each Figure, (a) is an optical micrograph showing the grain structure and general texture over a broad area of the surface and (b) - (e) are scanning electron micrographs showing electrode surfaces in the case of polished, etched, polished amalgamated, and etched amalgamated specimens, respectively.

Figures (1 - 3) (a) illustrate the influence of alloying on the grain size. Although additions of Pb and Cd do not appear to affect this to any appreciable extent, the addition of Fe clearly reduces the grain size by well over an order of magnitude.

A comparison of Figs. (1 - 3) (b) and (c) reveals the effect of etching. Clearly, there is a considerable increase in surface roughness on all specimens, as would be expected, but other deductions can be made. In the case of the Zn–Pb–Cd alloy it is clear that the segregation of components other than Zn occurs (*cf.* Figs. 2(c) and 1(c)), and these seem to be concentrated at grain (or sub-grain) boundaries. Judging by the alloy composition it was thought that this was predominantly Pb. This was confirmed by electron-probe microanalysis which also revealed the presence of Cd. It is therefore possible that the particles consist of a Pb–Cd alloy, although further work would be necessary to elucidate this point in more detail. In the case of the Zn–Pb–Cd–Fe alloy, however, the situation is much less well defined (Fig. 3(c)) although qualitatively similar. Despite the fact that Fe would be

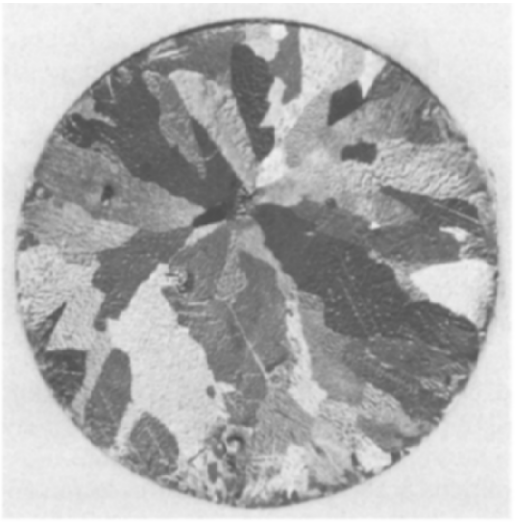

(a)

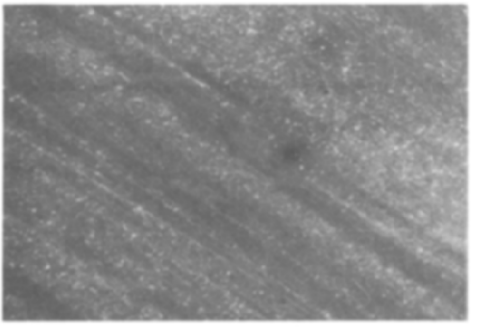

(b)

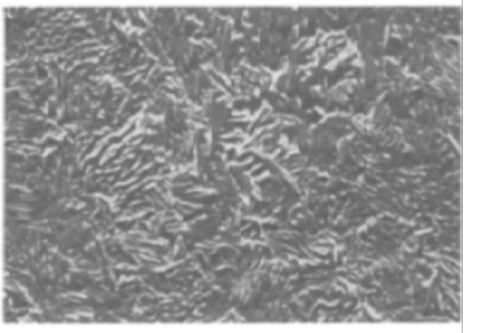

(c)

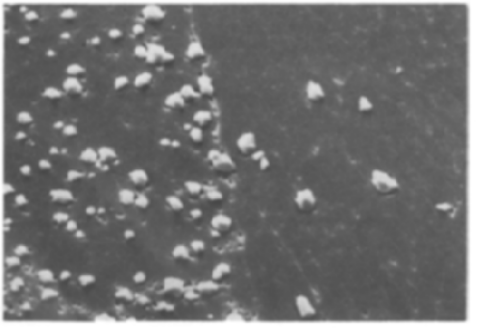

(d)

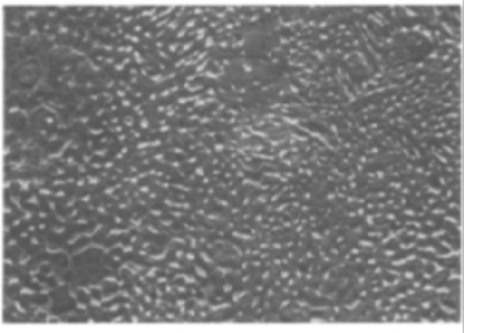

(e)

Fig. 1. Optical and scanning electron micrographs of pure Zn electrode surfaces. (a) Optical micrograph (×11) showing entire electrode area and grain structure after etching; (b)-(e) SEMS (×750) showing; (b) polished surface; (c) etched surface; (d) polished, amalgamated surface; (e) etched, amalgamated surface.

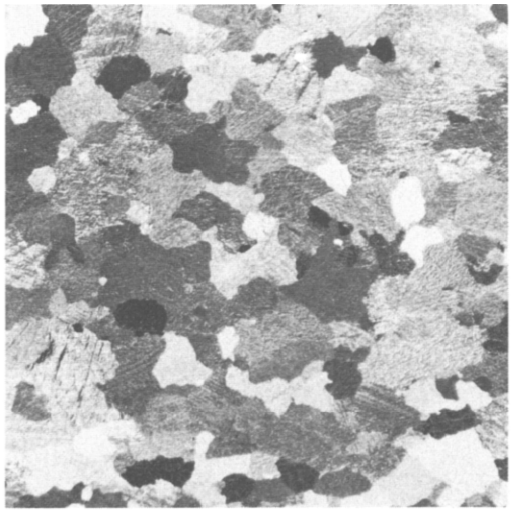

(a)

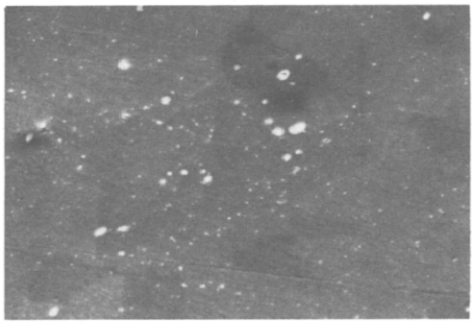

(b)

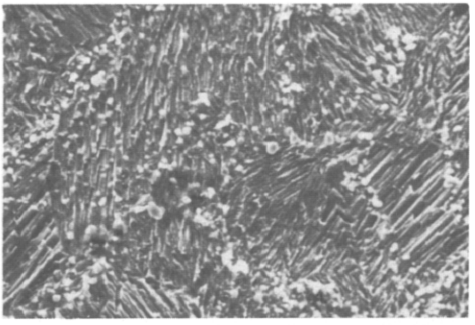

(c)

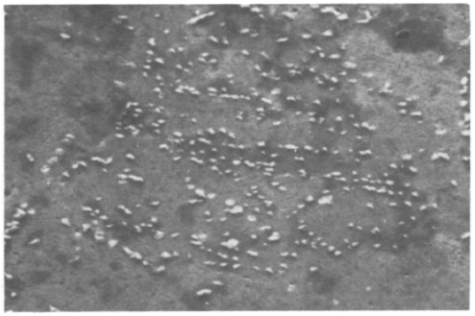

(d)

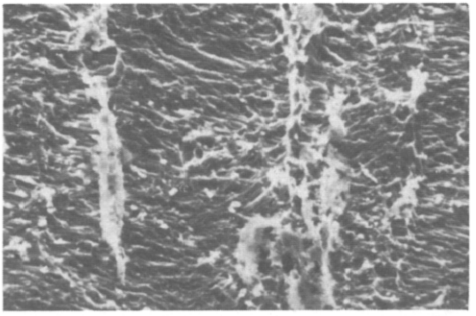

(e)

Fig. 2. Optical and scanning electron micrographs of Zn–Pb–Cd electrode surfaces. (a) Optical micrograph (×11) showing electrode grain structure after etching; (b) - (e) SEMS (×750) showing: (b) polished surface; (c) etched surface; (d) polished, amalgamated surface; (e) etched, amalgamated surface.

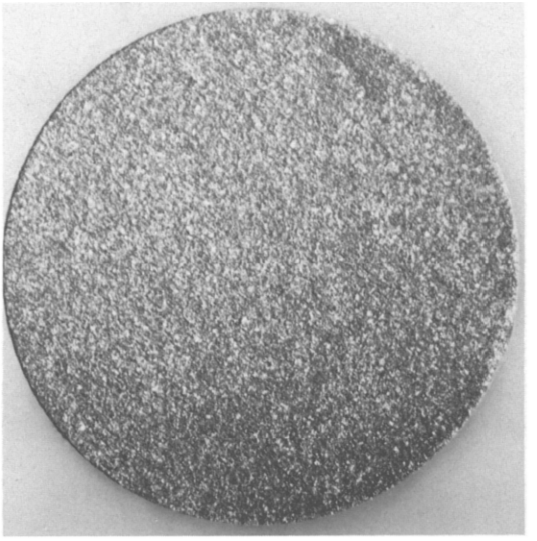

(a)

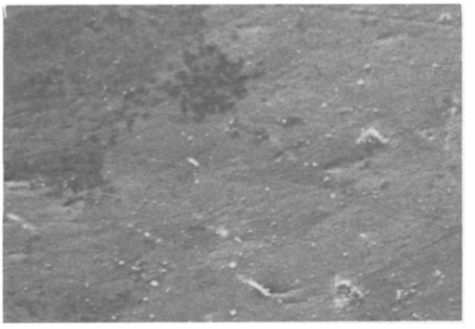

(b)

(c)

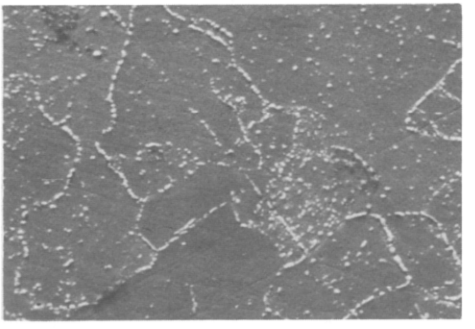

(d)

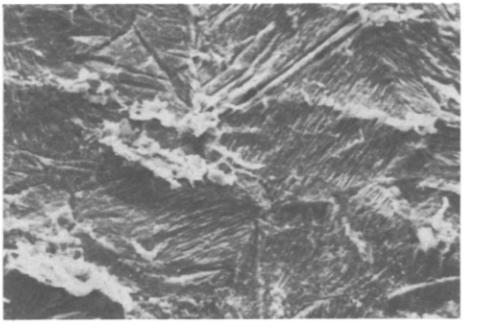

(e)

Fig. 3. Optical and scanning electron micrographs of Zn–Pb–Cd–Fe electrode surfaces. (a) Optical micrograph (×11) showing entire electrode area and grain structure after etching; (b) - (e) SEMS (×750) showing: (b) polished surface; (c) etched surface; (d) polished, amalgamated surface; (e) etched, amalgamated surface.

expected to be segregated at grain (or sub-grain) boundaries a large number of particles consisted of Pb/Cd.

A comparison of Figs. (1 - 3) (b) and (d) reveals the effect of amalgamating the *polished* electrode surfaces. In all cases it can be seen that the deposit appears to be localised. These results indicate that deposition occurs by a mechanism involving progressive nucleation and growth of three dimensional centres which would overlap to produce a coherent amalgam layer if larger quantities of mercury had been employed [5, 6].

In the case of pure zinc, deposition occurs preferentially onto certain grains (Fig. 1(d)). In the case of the Zn–Pb–Cd–Fe alloy, however, it is clear that grain boundary deposition is preferred (Fig. 3(d)). The Zn–Pb–Cd situation appears to be intermediate (Fig. 2(d)). It is important to note that in the region between the visible deposits the zinc is not devoid of mercury. It has been postulated from electrochemical evidence that a solid solution of Hg in Zn is formed (the α phase) which penetrates below the surface to the extent of several monolayers [1]. Thus, it is likely that the appearance of gross localised deposits only occurs after some saturation of the zinc surface region by the α phase has been accomplished.

A comparison of Figs. (1 - 3) (c) and (e) illustrates the effect of amalgamating the *etched* electrode surfaces. In contrast to the situation on the polished surfaces, mercury deposition is considerably less localised. This effect is demonstrated very clearly in the case of pure zinc from a comparison of Fig. 1(d) and (e). Observation of etched, amalgamated, pure zinc at higher magnifications (×5000) confirmed that the deposits were, indeed, localised, but that the number of nuclei had increased by well over an order of magnitude. A comparison of Figs. (2, 3) (c) and (e), however, shows that this deduction does not appear to apply in the case of the Zn–Pb–Cd and Zn–Pb–Cd–Fe alloys, where there is no evidence of localisation. All that can be concluded is that amalgamation induces a redistribution in, and possibly a modification to, the layer of accumulated minor alloying constituents.

(ii) Anodic dissolution characteristics

Figures 4 and 5 display the anodic branches of the current–potential curves for dissolution of the various metals for the different surface conditions. Figure 4(a) shows the effect of etching the unamalgamated polished electrodes, Fig. 4(b) the effect of amalgamating the polished electrodes, Fig. 5(a) the effect of amalgamating the etched electrodes and Fig. 5(b) the effect of pre-etching on the behaviour of the amalgamated electrodes. The anodic slopes are very similar and lie in the range 25 - 32 mV per decade, with a mean value of 28 mV per decade. This is very close to the theoretically predicted value of 30 mV per decade (2.3 $RT/2F$) indicative of a solution controlled (Nernstian) 2 electron exchange process. Thus, for a given electrode material (or range of alloys which differs in its composition to only a limited extent), the rate of dissolution is determined by the rate of diffusion of soluble zinc products away from the electrode surface.

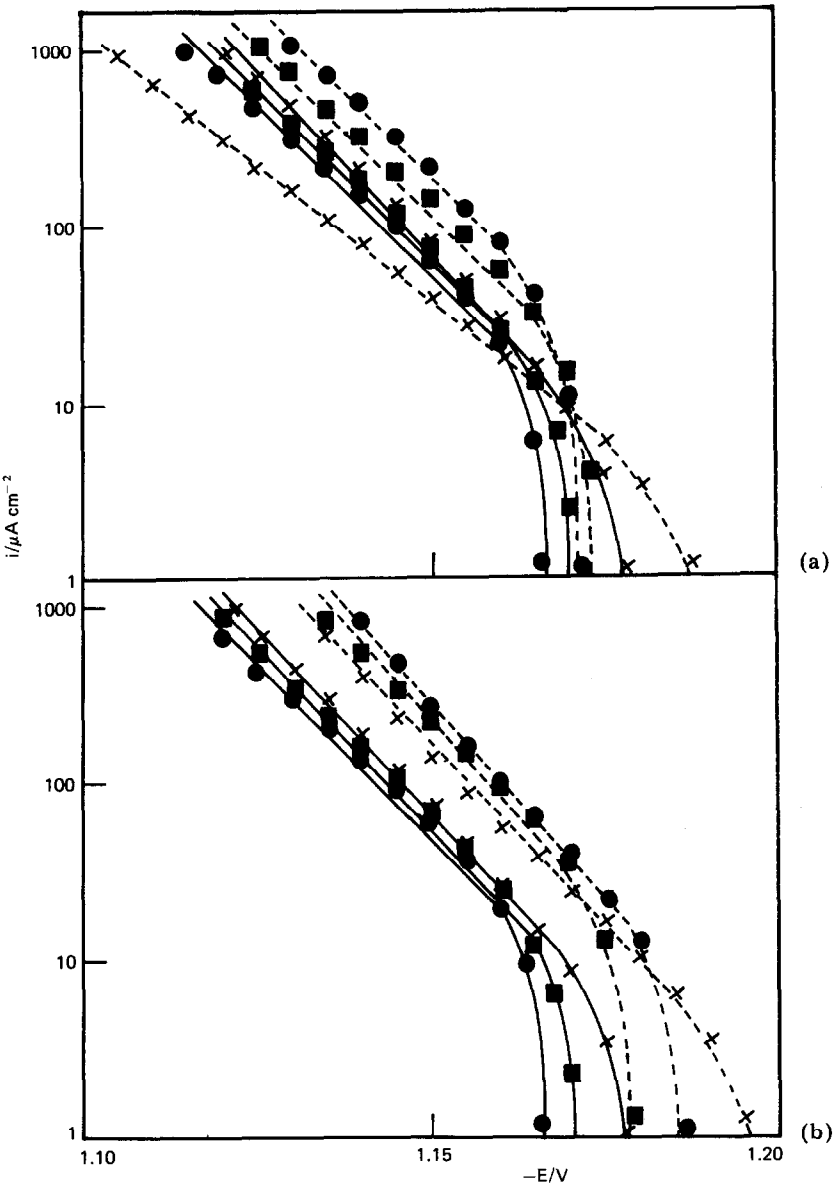

Fig. 4. (a) Anodic polarisation characteristics in 6.0 mol dm^{-3} NH_4Cl showing the effect of etching on the unamalgamated electrodes. ●, Pure Zn; ×, Zn–Pb–Cd alloy; ■, Zn–Pb–Cd–Fe alloy. ——, Polished surfaces; - - - -, etched surfaces. (b) Anodic polarisation characteristics in 6.0 mol dm^{-3} NH_4Cl showing the effect of amalgamation on the polished electrodes. ●, Pure Zn; ×, Zn–Pb–Cd; ■, Zn–Pb–Cd–Fe. ——, Unamalgamated surfaces; - - - -, amalgamated surfaces.

Despite the similarities in the *slopes* of the polarisation curves depicted in Figs. 4 and 5, it is clear that considerable variations in the *magnitude* of the dissolution current occur. In order to clarify the situation and to

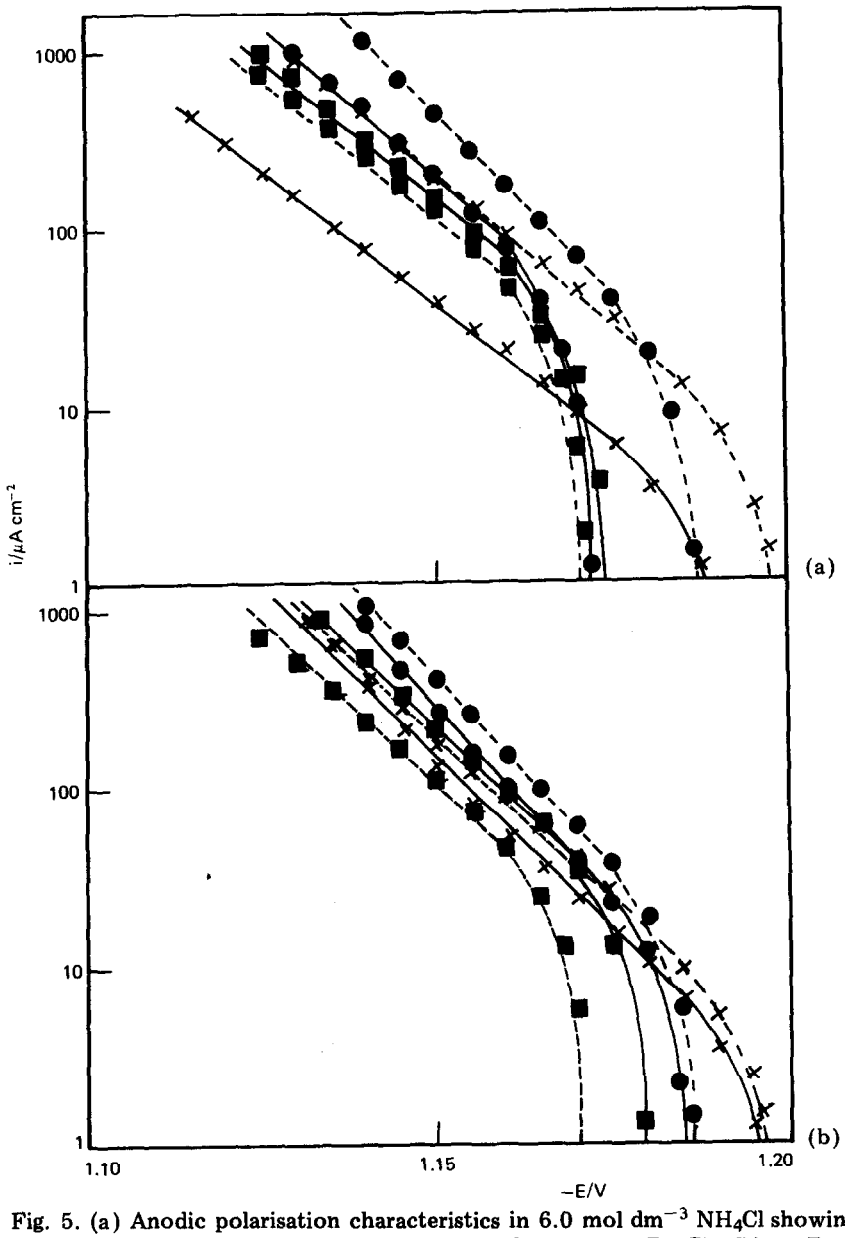

Fig. 5. (a) Anodic polarisation characteristics in 6.0 mol dm^{-3} NH_4Cl showing the effect of amalgamation on the etched electrodes. ●, Pure Zn; ×, Zn–Pb–Cd; ■, Zn–Pb–Cd–Fe. ——, Unamalgamated surfaces; - - - -, amalgamated surfaces. (b) Anodic polarisation characteristics in 6.0 mol dm^{-3} NH_4Cl showing the effect of pre-etching on the amalgamated electrodes. ●, Pure Zn; ×, Zn–Pb–Cd; ■, Zn–Pb–Cd–Fe. ——, Polished electrodes; - - - -, etched electrodes.

quantify the increases or decreases in the dissolution current, Table 1 summarises the trends in the form of anodic current ratios determined at −1.14 volts. The observations in Table 1 can be explained with the aid of

TABLE 1

Dissolution current ratios showing the effect of etching and amalgamation

Metal or alloy	Ratio 1 i_E/i_P unamalgamated	Ratio 2 i_A/i_U polished	Ratio 3 i_A/i_U etched	Ratio 4 i_E/i_P amalgamated
Zn	2.9	5.5	2.7	1.4
Zn–Pb–Cd	0.5	1.8	4.2	1.2
Zn–Pb–Cd–Fe	2.2	3.4	0.8	0.5

E = etched, P = polished, A = amalgamated, U = unamalgamated.

information gained from the analysis of the micrographs of Figs. 1 - 3, discussed previously. This explanation follows.

Figure 4(a) illustrates the effect of *etching* on the dissolution characteristics of the unamalgamated metals and the results are summarised in Ratio 1 of Table 1. As can be seen from the electron micrographs of Figs. (1 - 3) (b) and (c), a considerable increase in surface roughness is produced, as expected. In the case of pure zinc (Fig. 1(b) and (c)), an increase in the dissolution current by a factor of about 3 is clearly evident from Table 1, which can be correlated directly with the increase in the roughness factor for this electrode. Increases of a similar magnitude would be expected for the etched alloys. Double layer capacitance measurements determined for polished, pure zinc [5] indicate that the roughness factor is about 2.5. Thus, it can be deduced that the etched analogue has a roughness factor of about 7.5. Despite this, however, the dissolution current for the Zn–Pb–Cd alloy *decreases* significantly as a result of etching ($i_E/i_P = 0.5$). This can be attributed to a considerable "blocking" action achieved by the accumulation of Pb, or Pb(Cd) particles (Fig. 2(c)).

It is interesting to note that this effect, although present, is very much less severe in the case of the Zn–Pb–Cd–Fe alloy, where the anodic current ratio i_E/i_P is 2.2, which is closer to that of pure zinc. This suggests that it is the Pb content which is important in this respect since this differs by a factor of 4 in the two alloys, whereas the Cd contents are approximately equal (see Experimental section).

Figure 4(b) shows the effect amalgamation has on the discharge characteristics of the *polished* electrodes and the results are summarised in Ratio 2 of Table 1. It is clear that the dissolution curves for the unamalgamated metals are virtually identical, as would be expected, since the polished surfaces are clean and devoid of any accumulation of minor alloying constituents. Amalgamation produces a significant increase in the dissolution current on all electrodes. This, however, is largest for pure zinc ($i_A/i_U = 5.5$) and smallest for the Zn–Pb–Cd alloy ($i_A/i_U = 1.8$) with the Zn–Pb–Cd–Fe alloy being intermediate ($i_A/i_U = 3.4$). Again, these results suggest that it is the lead content which is important. Thus, the *activating* effect of Hg on zinc dissolution is apparently reduced by the presence of Pb within the alloy structure.

Although this activating effect of mercury is conclusively demonstrated in the present paper, and has been shown previously [5, 6], the exact mechanism of this process is unknown. Nevertheless, it is clear that very small quantities of mercury ($\leqslant 10$ μg cm^{-2}) produce very large, almost an order of magnitude, increases in zinc dissolution current. These results suggest that the activation energy for zinc dissolution is considerably less from a mercury-in-zinc solid solution than it is from the pure metal.

Figure 5(a) illustrates the effect of amalgamation on the dissolution characteristics of the *etched* metals and the results are summarised in Ratio 3 of Table 1. On etched, pure zinc amalgamation increases the anodic dissolution current by a factor of 2.7, which is only half that for the polished analogue (5.5). The reason for this becomes clear from a comparison of the micrographs in Fig. 1(b) and (d) and Fig. 1(c) and (e). The geometrical area of the polished electrode is considerably increased as a result of amalgamation whereas that of the etched electrode appears to be little changed. The effect of amalgamation on the dissolution current of etched pure zinc ($i_A/i_U = 2.7$) contrasts with that observed in respect of the Zn–Pb–Cd alloy ($i_A/i_U = 4.2$) and the Zn–Pb–Cd–Fe alloy ($i_A/i_U = 0.8$). These results can be understood when it is remembered that the etched alloy surfaces are covered with an adhered layer of the minor alloying constituents Pb, Cd and Fe. In the case of the Zn–Pb–Cd alloy it can be assumed that Pb and Cd are partially removed into a surface amalgam phase, thereby permitting far greater discharge currents than would otherwise occur. In the case of the Zn–Pb–Cd–Fe alloy it can be assumed that the surface is also *deactivated* with respect to the accumulation of Pb and Cd. Since the latter alloy also contains Fe, which does not form an amalgam, however, then the Fe particles will still provide a blocking action to zinc dissolution which cannot be removed by amalgamation, and the dissolution current will remain largely unchanged. These results provide further proof that the effect of amalgamation on zinc dissolution is conditioned by small changes in the composition of the alloy both for polished and etched electrodes.

Figure 5(b) shows the effect of *pre-etching* on the discharge characteristics of amalgamated electrodes and the results are summarised in Ratio 4 of Table 1. Comparing Fig. 5(b) with Figs. 4(a), (b), and 5(a), reveals the closeness of the curves, reflecting the fact that the amalgamation process has the effect of removing dissimilarities caused by the presence of the alloying constituents which participate as discussed previously.

(iii) Cathodic hydrogen-overvoltage characteristics

Figures 6 and 7 display the cathodic branches of the current–potential curves for hydrogen evolution on the various metals for the different surface conditions. Figure 6(a) shows the effect of etching the unamalgamated, polished electrodes, Fig. 6(b) the effect of amalgamating the polished electrodes, Fig. 7(a) the effect of amalgamating the etched electrodes, and Fig. 7(b) the effect of pre-etching on the behaviour of the amalgamated

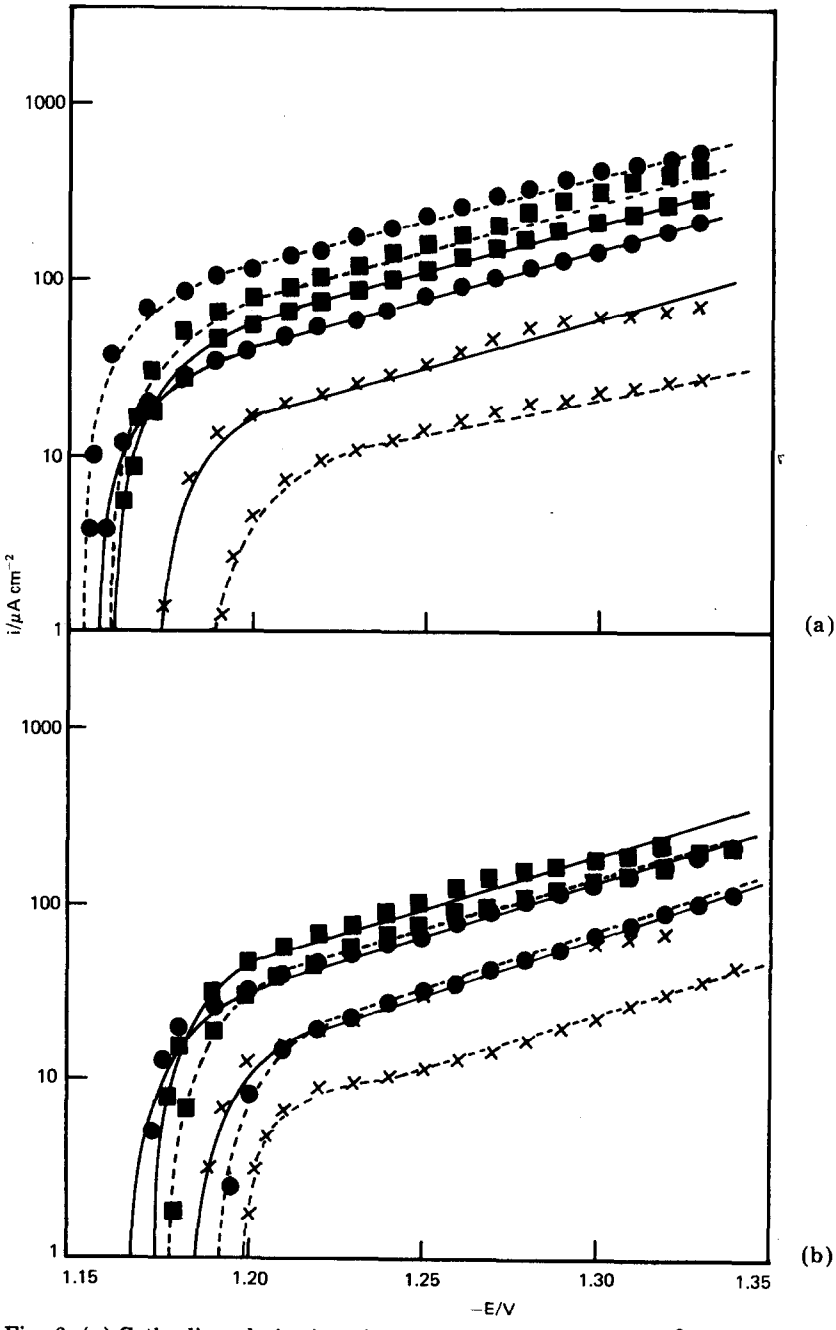

Fig. 6. (a) Cathodic polarisation characteristics in 6.0 mol dm^{-3} NH_4Cl showing the effect of etching on the unamalgamated electrodes. ●, Pure Zn; ×, Zn–Pb–Cd alloy; ■, Zn–Pb–Cd–Fe alloy. ——, Polished surfaces; - - - -, etched surfaces. (b) Cathodic polarisation characteristics in 6.0 mol dm^{-3} NH_4Cl showing the effect of amalgamation on the polished electrodes. ●, Pure Zn; ×, Zn–Pb–Cd; ■, Zn–Pb–Cd–Fe. ——, Unamalgamated surfaces; - - - -, amalgamated surfaces.

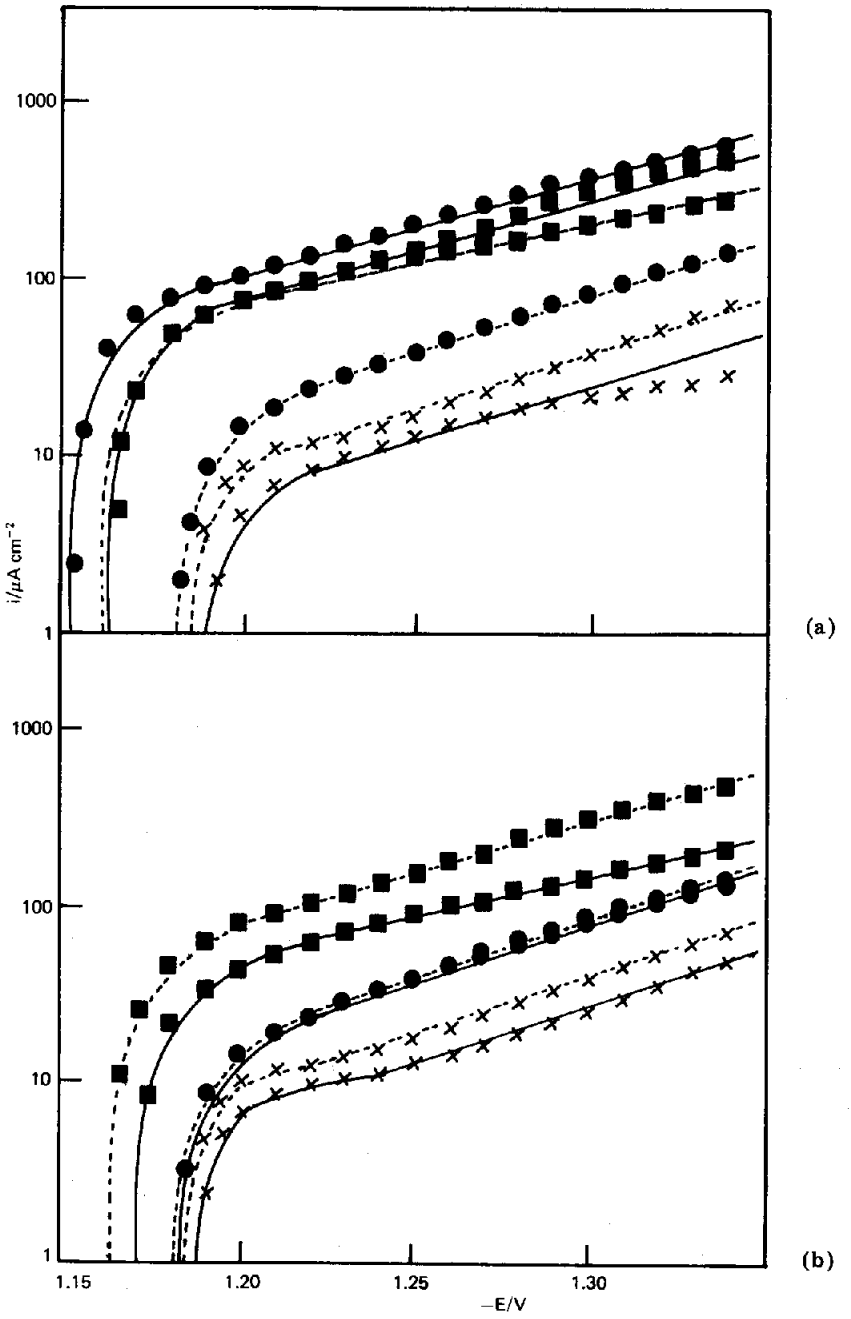

Fig. 7. (a) Cathodic polarisation characteristics in 6.0 mol dm^{-3} NH_4Cl showing the effect of amalgamation on the etched electrodes. ●, Pure Zn; ×, Zn–Pb–Cd; ■, Zn–Pb–Cd–Fe. ——, Unamalgamated surfaces; - - - -, amalgamated surfaces. (b) Cathodic polarisation characteristics in 6.0 mol dm^{-3} NH_4Cl showing the effect of pre-etching on the amalgamated electrodes. ●, Pure Zn; ×, Zn–Pb–Cd; ■, Zn–Pb–Cd–Fe. ——, Polished electrodes; - - - -, etched electrodes.

electrodes. The cathodic slopes are, in general, very similar, with mean values for each metal lying in the range 156 - 164 mV per decade when the anomalous slope for the etched, amalgamated Zn–Pb–Cd–Fe electrode (230 mV per decade) is removed from the analysis. These values are very similar to those observed previously for both amalgamated (20 $\mu g\ cm^{-2}$) and unamalgamated, pure zinc electrodes, and may be interpreted in terms of a predominantly charge-transfer controlled hydrogen evolution process involving the reduction of ammonium ions [6]. Despite the similarities in the *slopes* of the polarisation curves depicted in Figs. 6 and 7, very considerable variations in the *magnitude* of the hydrogen evolution current occurs. These trends are similar to those observed for zinc dissolution.

Table 2 summarises the cathodic polarisation characteristics in the form of current ratios determined at −1.155 volts by extrapolation. (This procedure was adopted in order that the ratios were determined at a potential close to the corrosion value, thus making them more relevant than those determined at higher cathodic potentials where changes can be expected due to variations in Tafel slope.) As with Table 1, the observations in Table 2 can also be explained with the aid of information gained from the analysis of the micrographs of Figs. 1 - 3, discussed previously.

TABLE 2

Hydrogen evolution current ratios showing the effect of etching and amalgamation

Metal or alloy	Ratio 1 i_E/i_P unamalgamated	Ratio 2 i_A/i_U Polished	Ratio 3 i_A/i_U Etched	Ratio 4 i_E/i_P Amalgamated
Zn	3.0	0.5	0.2	1.0
Zn–Pb–Cd	0.4	0.3	1.3	1.4
Zn–Pb–Cd–Fe	1.4	0.8	1.2	2.2

E = etched, P = polished, A = amalgamated, U = unamalgamated.

Figure 6(a) indicates that the magnitude of the hydrogen evolution current on the polished electrodes differs widely, being in the order:

$$Zn–Pb–Cd–Fe > Zn \gg Zn–Pb–Cd \quad (1)$$

From this sequence it can be deduced that the inhibiting effect of Pb and Cd on the rate of hydrogen evolution is heavily outweighed by the accelerating effect of Fe, despite its relatively smaller concentration. The ratio of the rates of hydrogen evolution on the three metals is 2.8:2.3:1 in sequence (1). Thus the capability of the Zn–Pb–Cd–Fe alloy to evolve hydrogen is almost 3 times as large as that for the Zn–Pb–Cd alloy. These differences are attributable to *catalytic* effects of the minor constituents on the rate of hydrogen evolution.

Figure 6(a) also illustrates the effect *etching* has on the hydrogen evolution characteristics of the unamalgamated metals, and the results are

summarised in Ratio 1 of Table 1. As can be seen from the electron micrographs of Figs. (1 - 3) (b) and (c), a considerable increase in surface roughness is produced. In the case of pure zinc, an increase in the rate of hydrogen evolution by a factor of 3.0 is shown in Table 2 which can be correlated with the increase in the roughness factor of the electrode. This value is almost identical with that obtained from a consideration of changes in the zinc dissolution current for pure zinc (Ratio 1, Table 1). Increases of a similar order would be expected for the etched alloys.

Despite this, however, the hydrogen evolution current for the Zn–Pb–Cd alloy *decreases* significantly as a result of etching ($i_E/i_P = 0.4$). This demonstrates that any increases in current resulting from area changes are heavily outweighed by the surface accumulation of Pb or Pb (Cd) particles which reduce the current as a consequence of both a blocking action and by reducing the catalytic activity of the zinc with respect to hydrogen evolution.

In the case of the Zn–Pb–Cd–Fe alloy, however, the rate of hydrogen evolution is not significantly affected by etching. The factors which influence the ratio for this alloy are more numerous. Thus, it is possible that the effect of the increase in electrode area, in addition to the increase in surface Fe content, is almost counterbalanced by the blocking action of Pb or Pb (Cd) particles and their reduced catalytic activity with respect to hydrogen evolution. Such a situation is complex and beyond further resolution at present.

Figure 6(b) shows the effect amalgamation has on the hydrogen evolution characteristics of the *polished* metals and the results are summarised in Ratio 2 of Table 2. It can be seen that the efficiency with which amalgamation reduces hydrogen evolution decreases in the order:

$$\text{Zn–Pb–Cd} > \text{Zn} > \text{Zn–Pb–Cd–Fe} \qquad (2)$$

The efficiency values are 68%, 54% and 24%, respectively. The relatively greater effectiveness of mercury for reducing hydrogen evolution on the Zn–Pb–Cd alloy, compared with that on pure zinc, may be attributed to a more even distribution of mercury on the former, perhaps facilitated by the presence of the minor alloying constituents in which mercury is more soluble (*cf.* Figs. (1 - 3) (d)). The poorer effectiveness of mercury for reducing hydrogen evolution on the Zn–Pb–Cd–Fe electrode can be attributed to the fact that the gas is evolved, in part, from Fe inclusions which are not amalgamated. The sum total of these effects is that the amalgamated Zn–Pb–Cd–Fe alloy is capable of producing about 7 times more hydrogen than the amalgamated Zn–Pb–Cd alloy under similar conditions.

Figure 7(a) illustrates the effect amalgamation has on the cathodic polarisation characteristics for the *etched* metals and the results are summarised in Ratio 3 of Table 2. It is clear that for etched, pure zinc, amalgamation is highly effective in reducing hydrogen evolution and considerably more so than on the polished surface (*cf.* Ratios 2 and 3). The hydrogen evolution inhibiting efficiency of mercury on the etched surface is 85% compared with only 54% on the polished analogue. This result can be explained

by the mercury both reducing the surface roughness of the etched electrode and also acting as inhibitor (*cf.* Fig. 1(d) and (e)). These results contrast sharply with those for the Zn–Pb–Cd and Zn–Pb–Cd–Fe alloys, where it appears that mercury accelerates the gassing rate (i_A/i_U = 1.3 and 1.2, respectively).

The results can be explained if it is assumed that the Pb or Pb (Cd) layer formed on the alloys as a result of etching is at least as effective as mercury as an inhibitor, since the hydrogen overvoltages of these metals are of a very similar order. The slight acceleration in the rate of hydrogen evolution can be explained in terms of the partial removal of this layer and subsequent loss of protection.

Figure 7(b) shows the effect *pre-etching* has on the polarisation characteristics of the amalgamated electrodes and the results are summarised in Ratio 4 of Table 2. In the case of pure zinc it is conspicuous that the curves are coincident, reflecting the ability of mercury to remove surface roughness induced by etching, as discussed previously. Despite this, however, the rate of hydrogen evolution on the etched, amalgamated Zn–Pb–Cd–Fe electrode, in particular, is considerably higher than that on the polished analogue (i_E/i_P = 2.2). It is clear from the preceding discussion that this is due to the accumulation of Fe particles of low hydrogen overvoltage on the alloy surface during etching which cannot be removed by amalgamation. The deleterious effect of Fe in the alloy composition is shown clearly in Fig. 7(b), where it can be seen that very large variations of almost an order of magnitude exist for the hydrogen evolution rate on the etched electrodes.

The order is:

$$\text{Zn–Pb–Cd–Fe} \gg \text{Zn} \gg \text{Zn–Pb–Cd} \qquad (3)$$

(iv) Summary of corrosion rates

Tables 3 - 5 summarise the important corrosion parameters obtained on the three electrodes for all surface conditions. The corrosion currents are quoted in respect of both Tafel line extrapolation (i_{corr}^{Ext}) and polarisation resistance ($i_{corr}^{R_p}$) methods. Figure 8(a) - (c) summarises the linear polarisation plots in the vicinity of the corrosion potential from which the R_p values were deduced. A comparison of corrosion currents obtained on repeat experiments shows that, in general, reproducibility is quite good. Also, the agreement between i_{corr}^{Ext} and $i_{corr}^{R_p}$ values provides further confidence for the quoted parameters.

Tables 6 and 7 provide more insight into the effect of the specific surface changes on the corrosion rate of the various metals. The quoted parameters were derived from i_{corr}^{GM} values taken from Tables 3 - 5. It must be emphasised, however, that since the corrosion currents contain contributions from both the anodic and cathodic polarisation characteristics discussed earlier, no *original* information concerning the nature and rate of these electrode processes can be obtained from additional analysis. Furthermore, it is primarily the rate of hydrogen evolution which determines the corrosion

TABLE 3

Corrosion data for pure zinc

Surface condition	E_{corr} (V *vs.* SCE)	b_c (mV)	b_a (mV)	R_p (Ω cm^2)	$i_{corr}^{R_p}$ (μA cm^{-2})	i_{corr}^{Ext} (μA cm^{-2})	i_{corr}^{M} (μA cm^{-2})	i_{corr}^{GM} (μA cm^{-2})
Polished unamalgamated	−1.158	176	30	511	21.8	25.0	24.6 (R_p)	24.3
	−1.159	170	31	418	27.3	23.0	24.0 (Ext)	
Etched unamalgamated	−1.157	146	28	150	68	63	67 (R_p)	62.5
	−1.154	156	26	146	66	53	58 (Ext)	
Polished amalgamated	−1.184	149	24	548	16.4	14.3	15.7 (R_p)	15.4
	−1.186	150	24	604	14.9	16.1	15.2 (Ext)	
Etched amalgamated	−1.185	148	25	434	21.4	19.0	20.9 (R_p)	19.1
	−1.187	152	25	458	20.4	15.3	17.2 (Ext)	

$i_{corr}^{R_p}$ = Corrosion current from R_p and b values (Stern–Geary).
i_{corr}^{Ext} = Corrosion current from Tafel Line extrapolation to E_{corr}.
i_{corr}^{M} = Mean corrosion current from R_p or Ext methods.
i_{corr}^{GM} = Grand mean corrosion current from R_p and Ext methods.

TABLE 4

Corrosion data for Zn–Pb–Cd alloy

Surface condition	E_{corr} V *vs.* SCE	b_c (mV)	b_a (mV)	R_p (Ω cm^2)	$i_{corr}^{R_p}$ (μA cm^{-2})	i_{corr}^{Ext} (μA cm^{-2})	i_{corr}^{M} (μA cm^{-2})	i_{corr}^{GM} (μA cm^{-2})
Polished unamalgamated	−1.175	159	30	1120	9.8	14.2	11.8 (R_p)	14.1
	−1.170	172	29	782	13.8	18.6	16.4 (Ext)	
Etched unamalgamated	−1.183	180	32	2625	4.5	3.8	4.0 (R_p)	4.0
	−1.189	180	28	3099	3.4	4.4	4.1 (Ext)	
Polished amalgamated	−1.188	161	24	1316	6.9	5.6	6.3 (R_p)	6.0
	−1.192	164	24	1625	5.6	6.0	5.8 (Ext)	
Etched amalgamated	−1.185	150	29	1447	7.3	6.2	8.9 (R_p)	7.6
	−1.186	150	31	1074	10.4	6.2	6.2 (Ext)	

$i_{corr}^{R_p}$ = Corrosion current from R_p and b values (Stern–Geary).
i_{corr}^{Ext} = Corrosion current from Tafel Line extrapolation to E_{corr}.
i_{corr}^{M} = Mean corrosion current from R_p or Ext methods.
i_{corr}^{GM} = Grand mean corrosion current from R_p and Ext methods.

TABLE 5

Corrosion data for Zn–Pb–Cd–Fe alloy

Surface condition	E_{corr} V *vs.* SCE	b_c (mV)	b_a (mV)	R_p (Ω cm^2)	i_{corr}^{Rp} (μA cm^{-2})	i_{corr}^{Ext} (μA cm^{-2})	i_{corr}^{M} (μA cm^{-2})	i_{corr}^{GM} (μA cm^{-2})
Polished unamalgamated	−1.165	145	28	433	25.5	30.0	22.4 (R_p)	25.2
	−1.169	147	26	504	19.3	26.0	28.0 (Ext)	
Etched unamalgamated	−1.164	180	28	231	49.0	53.0	44.0 (R_p)	44.5
	−1.166	173	28	288	39.0	37.0	45.0 (Ext)	
Polished amalgamated	−1.173	160	26	279	36.1	31.0	29.9 (R_p)	29.2
	−1.173	160	24	392	23.6	26.0	28.5 (Ext)	
Etched amalgamated	−1.166	230	32	283	54.8	60.0	52.8 (R_p)	52.9
	−1.166	230	32	248	50.7	46.0	53.0 (Ext)	

i_{corr}^{Rp} = Corrosion current from R_p and b values (Stern–Geary).
i_{corr}^{Ext} = Corrosion current from Tafel Line extrapolation to E_{corr}.
i_{corr}^{M} = Mean corrosion current from R_p or Ext methods.
i_{corr}^{GM} = Grand mean corrosion current from R_p and Ext methods.

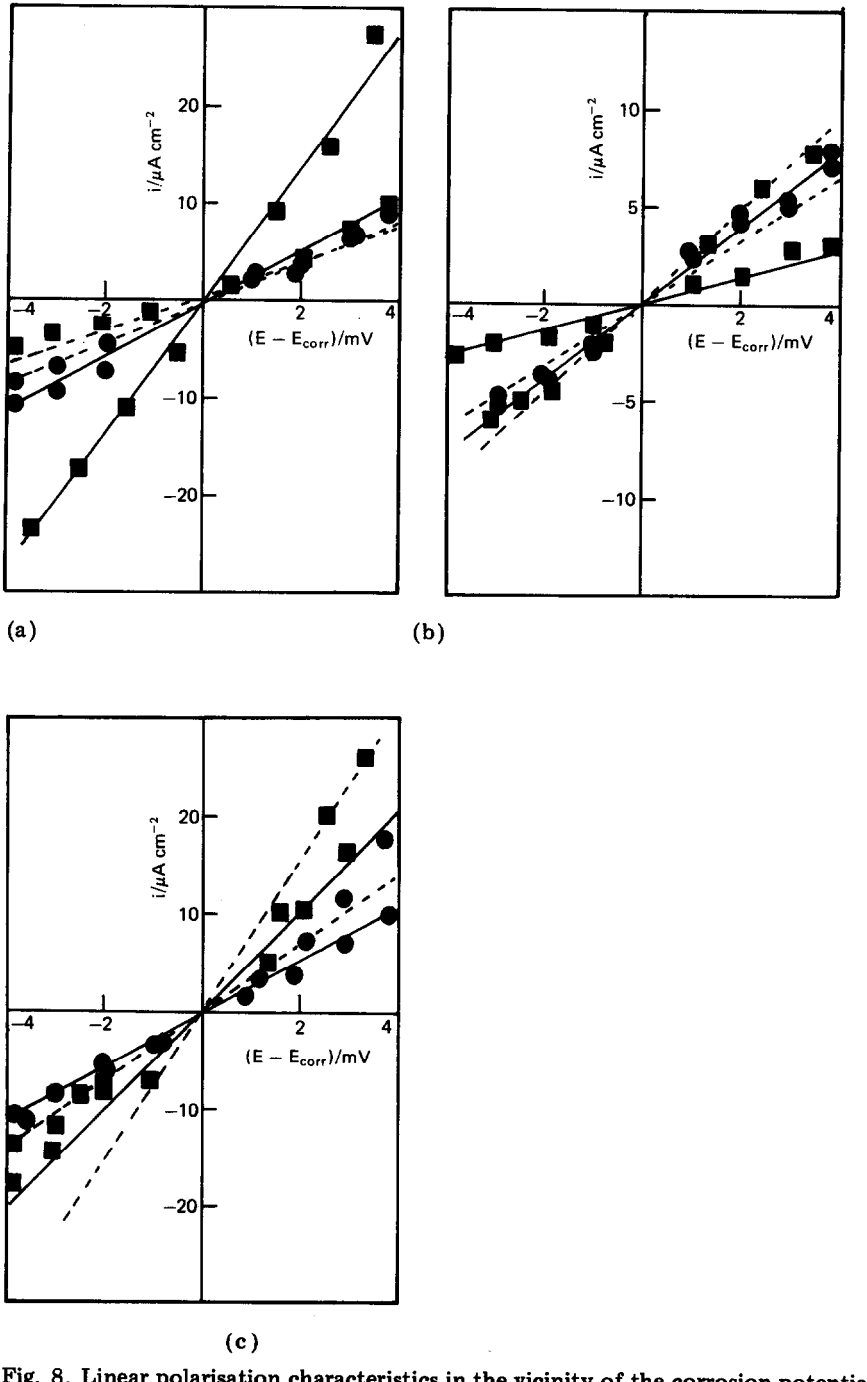

Fig. 8. Linear polarisation characteristics in the vicinity of the corrosion potential for: (a) pure zinc, (b) Zn–Pb–Cd alloy, (c) Zn–Pb–Cd–Fe alloy electrodes in 6.0 mol dm^{-3} NH_4Cl. ●——●, Polished, unamalgamated surface; ●- - -●, polished, amalgamated surface; ■——■, etched, unamalgamated surface; ■- - -■, etched, amalgamated surface.

TABLE 6

Effect of amalgamation on the corrosion rate

Surface preparation	Change in corrosion rate (%)		
	Zn	Zn–Pb–Cd	Zn–Pb–Cd–Fe
Polished	−37	−58	+16
Etched	−69	+90	+19

N.B. + signifies an increase.
− signifies a decrease.

TABLE 7

Effect of etching on the corrosion rate

Surface preparation	Change in corrosion rate (%)		
	Zn	Zn–Pb–Cd	Zn–Pb–Cd–Fe
Unamalgamated	+157	−72	+77
Amalgamated	+24	+27	+81

N.B. + signifies an increase.
− signifies a decrease.

rate since $b_C \gg b_a$ (cathodic control) and, therefore, a satisfactory explanation of the trends depicted in Tables 6 and 7 can only be obtained from a consideration of changes in the rate of this reaction. These changes and their causes have been discussed previously.

Conclusion

The present investigation highlights the extreme sensitivity of the polarisation characteristics of zinc to small changes in composition with respect to high (Pb and Cd) and low (Fe) hydrogen overvoltage components. It also emphasizes the need to examine different methods of electrode surface preparation if an understanding of the corrosion behaviour of zinc alloys in batteries is to be obtained.

In addition to its significance in the application of zinc as an anode material in battery systems, it is suggested that the information discussed in respect of zinc dissolution could also be of value in the field of cathodic protection using sacrificial zinc anodes.

Acknowledgements

The authors express their gratitude to Dr N. C. White for preparing both the diagrams and the metal specimens for photography. They also wish to thank Dr F. L. Tye for helpfully discussing aspects of this work during the experimental stage and the Directors of Ever Ready Limited for permission to publish.

References

1 L. M. Baugh, *Electrochim. Acta, 24* (1979) 657.
2 L. M. Baugh, *Electrochim. Acta, 24* (1979) 669.
3 L. M. Baugh, P. M. Gidney and J. A. Lee, *Electrochim. Acta, 25* (1980) 751.
4 L. M. Baugh, P. M. Gidney and J. A. Lee, *Electrochim. Acta, 25* (1980) 765.
5 L. M. Baugh, F. L. Tye and N. C. White, in J. Thomson (ed.), *Power Sources 9*, Academic Press, London, 1983, p. 303.
6 L. M. Baugh, F. L. Tye and N. C. White, *J. Appl. Electrochem., 13* (1983) 623.